ChemComm

COMMUNICATION

$FeSe_2$ films with controllable morphologies as efficient counter electrodes for dye-sensitized solar cells†

Cite this: DOI: 10.1039/c3cc49175g

Received 3rd December 2013, Accepted 10th January 2014

DOI: 10.1039/c3cc49175g

www.rsc.org/chemcomm

Wenjun Wang,[a] Xu Pan,*[a] Weiqing Liu,[a] Bing Zhang,[b] Haiwei Chen,[a] Xiaqin Fang,[a] Jianxi Yao[b] and Songyuan Dai*[ab]

The $FeSe_2$ films with controllable morphologies (including 3D flower-like and sphere-shaped) have been applied as the counter electrodes (CEs) for dye-sensitized solar cells (DSSCs). It is found that 3D flower-like $FeSe_2$ CEs perform comparably to conventional platinum CEs (power conversion efficiencies of 8.00 and 7.87%, respectively).

Dye-sensitized solar cells (DSSCs) are promising alternatives to conventional solid-state photovoltaic devices based on materials such as Si, CdTe and $CuIn_{1-x}Ga_xSe_2$, owing to their low cost, ease of production and high efficiency.[1] In general, a typical DSSC usually comprises three main components: a dye-sensitized porous nanocrystalline titanium dioxide (TiO_2) film as the photoanode, an electrolyte traditionally containing an iodide/triiodide (I^-/I_3^-) redox couple and a counter electrode (CE).

As a crucial component, CE plays an important role in the performance of a DSSC in that it collects electrons from external circuit and fulfills electron transfer from the CE interface to the electrolyte by catalyzing the reduction of I_3^- to I^-. Usually, fluorine doped tin oxide (FTO) glass loaded with noble metal platinum (Pt) is the preferred material for the CE due to its superior conductivity, electrocatalytic activity, and stability.[2] However, in view of the low abundance and high cost of platinum, much incentive exists in developing other cost-effective alternatives for Pt. For instance, carbon materials,[3] conducting polymers[4] and inorganic compounds[5,6] have been utilized as CEs in DSSCs. In particular, some metal chalcogenides among these Pt-free electrocatalysts have been shown to be quite effective and have exceeded the performance of Pt.[7–10] As another compound in the metal chalcogenide series, iron diselenide ($FeSe_2$) is an important VIII–VI transition metal selenide semiconductor and has drawn enormous attention owing to its unusual structure and electronic properties, as well as the opportunity it offers to engineer special shapes for application in the development of advanced functional devices. In recent years, much effort has been devoted to the synthesis of $FeSe_2$ films, low-dimensional $FeSe_2$ micro/nanostructures and anisotropic three-dimensional (3D) $FeSe_2$ nanostructures. However, to the best of our knowledge, no research on the use of $FeSe_2$ as CEs in DSSCs has been reported so far.

Herein, as the electrocatalytic activity may depend on the morphology, we have prepared the $FeSe_2$ films with controllable morphologies, including 3D flower-like $FeSe_2$ assembled with nano/microrods (F_r) and sphere-shaped $FeSe_2$ assembled with sphere-shaped particles (F_s), *via* a facile hydrothermal synthetic approach, and used them as Pt-free electrocatalysts for DSSCs, respectively. Electrochemical results of the F_r CE showed Pt-like catalytic activity for triiodide reduction, surpassing that of the F_s CE. As a result, the power conversion efficiency (η) of the DSSC with the F_r CE was 8.00%, which was comparable to that of the Pt CE (7.87%), while the η of the F_s CE was 7.38%. Details of the fabrication method are shown in the experimental section of the ESI.†

The crystallographic structures of the as-synthesized $FeSe_2$ products were characterized by X-ray diffraction (XRD). From the XRD patterns (Fig. 1), all diffraction peaks of F_r and F_s can be readily indexed to an orthorhombic phase of $FeSe_2$ (JCPDS No. 65-2570). The morphologies of the $FeSe_2$ samples (F_r and F_s) were observed using typical scanning electron microscopy (SEM) and transmission electron microscopy (TEM). As shown in Fig. 2a, the as-obtained F_r

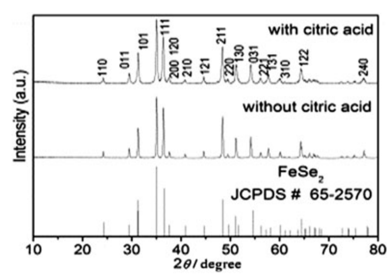

Fig. 1 XRD patterns of the as-synthesized $FeSe_2$ products.

[a] *Key lab of Novel Thin Film Solar Cells, Institute of Plasma Physics, Chinese Academy of Sciences, Hefei, PR China. E-mail: sydai@ipp.ac.cn, mars_dark@hotmail.com; Fax: +86 (0)551 5591377; Tel: +86 (0)551 5591377*

[b] *State Key Laboratory of Alternate Electrical Power System with Renewable Energy Sources, North China Electric Power University, Beijing 102206, China*

† Electronic supplementary information (ESI) available: Full experimental procedures. See DOI: 10.1039/c3cc49175g

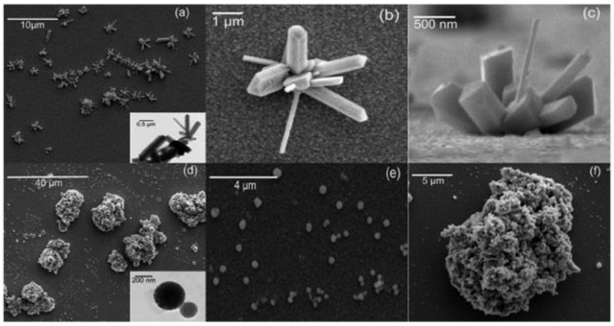

Fig. 2 (a) Low-, (b) high-magnification and (c) cross-section SEM images of F_r grown *in situ* on the FTO glass. The inset shows the TEM image of F_r. (d) Low and (e, f) high-magnification SEM images of F_s grown *in situ* on the FTO glass. The inset shows the TEM image of F_s.

CE in the reaction system without citric acid consists almost entirely of the flower-like $FeSe_2$ assembled with micro/nanorods with an average diameter of 0.5–3 μm. Only a small portion of single micro/nanorods can be found. As shown in Fig. 2(b) and (c), the 3D flower-like microconstruction is composed of many 1-dimensional sub-units (micro/nanorods) that connect with each other by self-assembly. The inset shows the TEM image of F_r. Fig. 2d shows the SEM image of the as-obtained F_s CE in the same reaction system with additional citric acid. The surface is partially covered with single relatively uniform sphere-shaped particles (Fig. 2e). Meanwhile, other parts of the film have large near-spherical particles. The sizes of the large near-spherical particles are found to be in micrometer-scale. As can be seen at higher magnification (Fig. 2f), the large near-spherical particles are composed of lots of nano-particles. The inset of Fig. 2d shows the TEM image of single sphere-shaped particles with a mean size of 200–400 nm.

The performances of the DSSCs with F_r and F_s CEs were studied in comparison to that of the DSSC with the Pt CE. The photo-current–voltage (I–V) curves of the DSSCs applying F_r, F_s and Pt CEs are shown in Fig. 3 (under simulated solar light illumination of 100 mW cm^{-2}). The corresponding photovoltaic parameters are summarized in Table 1. As shown in Table 1, when the F_r was used as the counter electrode, the DSSC exhibits a short-circuit current (J_{sc}) of 14.93 mA cm^{-2}, an open-circuit voltage (V_{oc}) of 744 mV, a fill factor (FF) of 0.721, and an η of 8.00%. The DSSC with the Pt CE, on the contrary, renders a J_{sc} of 15.13 mA cm^{-2}, a V_{oc} of 741 mV, a FF of 0.702 and an η of 7.87%. The F_r-based cells showed a comparable, even slightly higher, η than Pt, which is mainly attributed to the slight improvement in the FF. Meanwhile, the η of 7.38% has been obtained by the DSSCs applying F_s CEs, indicating a poorer catalytic

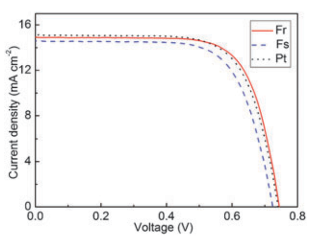

Fig. 3 I–V curves of DSSCs with F_r, F_s and Pt electrodes.

Table 1 Photovoltaic and EIS parameters of the DSSCs with different CEs

CEs	V_{oc}/ mV	J_{sc}/ mA cm^{-2}	FF	η/%	R_s/ Ω cm^2	R_{ct}/ Ω cm^2	Z_N/ Ω cm^2	E_{pp}/ mV
F_r	744	14.93	0.721	8.00	16.82	0.53	0.43	252
F_s	724	14.60	0.698	7.38	27.05	0.96	0.79	302
Pt	741	15.13	0.702	7.87	17.01	0.78	0.59	262

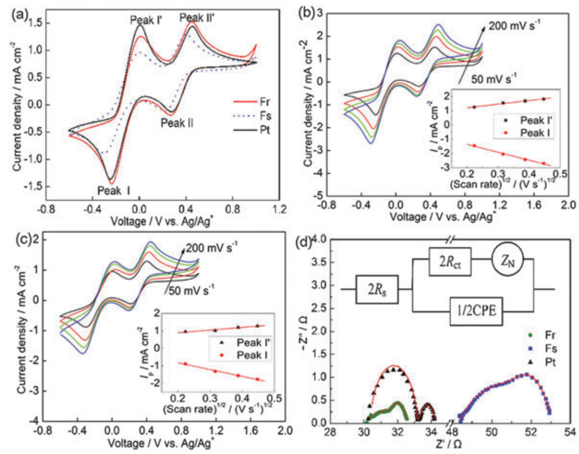

Fig. 4 (a) Cyclic voltammograms for F_r, F_s and Pt CEs obtained at a scan rate of 50 mV s^{-1}. (b, c) CV curves of the F_r and F_s CEs at various scan rates. The inset shows the redox peak current of eqn (1) as a function of scan rate. (d) Nyquist plots obtained by EIS analysis of the symmetrical cells. The inset gives the equivalent circuit.

activity for the reduction of I_3^-. The incident photon-to-current conversion efficiency (IPCE) spectra of these DSSCs were also collected (see ESI†).

To investigate the reaction kinetics of various electrodes in the I^-/I_3^- electrochemical system, cyclic voltammetry (CV) was carried out in a three-electrode system. Fig. 4(a) shows the CV curves of the F_r, F_s and Pt CEs, respectively. Two pairs of redox peaks (peak I/peak I′ and peak II/peak II′) are observed for all of the materials. The left redox peaks correspond to eqn (1) and the right ones correspond to eqn (2)[11,12]

$$I_3^- + 2e^- \leftrightarrow 3I^- \quad (1)$$

$$3I_2 + 2e^- \leftrightarrow 2I_3^- \quad (2)$$

Since the counter electrode of a DSSC is responsible for catalyzing the reduction of I_3^- to I^-, the characteristics of peak I and peak I′ are the focus of our analysis. The peak current and the peak-to-peak separation (E_{pp}), which is negatively correlated with the standard electrochemical rate constant of the redox reaction, are two critical parameters for comparing electrocatalytic activities of different CEs.[13]

As shown in Fig. 4(a), the lower E_{pp} and higher current densities of the F_r electrode indicate that F_r produces higher reversibility of the I_3^-/I^- redox reaction and remarkable electrocatalytic activity for I_3^- reduction, even better than Pt, which is advantageous for the application of the F_r electrode as an efficient CE in DSSCs. Meanwhile, the lower peak current densities and larger E_{pp} of the F_s electrode reveal that the electrocatalytic activity of the F_s electrode is inferior to that of F_r and Pt electrodes. The conclusion from the CV data is consistent with previous energy conversion efficiency results. The η of the F_s-based DSSCs are lower than those of F_r and Pt-based DSSCs, which stems from the inferior electrocatalytic ability of the F_s electrodes.

Fig. 4(b) and (c) represent the typical CV curves of F_r and F_s electrodes in the I^-/I_3^- system with different scan rates. As shown in Fig. 4(b) and (c), the peak current densities (I_p) changed with the scan rate. Also, the cathodic peaks gradually and regularly shifted negatively, and the corresponding anodic peaks shifted positively upon increasing the scan rate. The inset of Fig. 4(b) and (c) illustrates a linear relationship between the redox peak current density and the square root of scan rates. According to the Langmuir isotherms principle, this linear relationship indicates the diffusion limitation of the redox reactions (eqn (1)) on the surface of F_r and F_s CEs.[14] This phenomenon also shows that the adsorption of iodide species is little affected by the redox reaction on the surface of F_r and F_s CEs and there is no specific interaction between the I^-/I_3^- redox couple and F_r and F_s CEs as is the case of the Pt CE.[15,16]

To further elucidate the electrocatalytic activity of the $FeSe_2$ CEs in the reduction of I_3^- ions, electrochemical impedance spectroscopy (EIS) was conducted on the symmetrical F_r–F_r, F_s–F_s and Pt–Pt
Q7 electrochemical cells. Fig. 3(d) shows the Nyquist plots obtained by the EIS analysis of symmetric cells and the equivalent circuit diagram
Q8 used for the simulation. Generally, the high-frequency intercepts on the real axis represent the series resistance (R_s), which is mainly composed of the bulk resistance of CE materials, resistance of FTO glass substrates, contact resistance, *etc.* The high frequency semicircle indicates the electrochemical charge transfer resistance (R_{ct}) at the interface of CE/electrolyte for I_3^- reduction and the corresponding constant phase element (CPE) describing deviation from the ideal capacitance, due to the electrode roughness, whereas the low frequency semicircle indicates the Nernst diffusion-limited impedance (Z_n) of the I^-/I_3^- redox species in the electrolyte.[16] The Nyquist plots were fitted and the impedance parameters of various electrodes obtained by fitting are shown in Table 1. The F_r CE possessed the lowest R_{ct} (0.53 Ω cm^2), so it had a relatively high catalytic activity. The conclusions derived from the EIS and CV data are consistent. Furthermore, previous analyses have indicated that the total series resistance (R_{series}) of solar cells strongly influences the FF and η.[16,17] In DSSCs, the R_{series} is mainly related to R_s, R_{ct}, the diffusion impedance of I_3^- ions in the electrolyte and the electron transfer at the TiO_2/dye/electrolyte interface.[17] The lowest R_{ct}, R_s and Z_n of the F_r CE resulted in the minimum series resistance, and hence the F_r based device showed a corresponding improvement in the FF and η. Meanwhile, the R_s of F_s increased significantly compared to F_r, which also resulted in a lower electrocatalytic activity.

In addition, although the exact reason for the influence of morphology on the performance of $FeSe_2$ CEs is still unclear, the following points may be noted. In principle, the prerequisite for triiodide reduction is the adsorption of acceptor-like species (such as I_2 and I_3^-) at active sites of semiconductor catalysts ($FeSe_2$) through charge-transfer chemisorption.[16,18] Therefore, the performance of $FeSe_2$ CEs is sensitive to their surface structure. The 3D flower-like morphology may improve the total surface area exposed to the electrolyte, which may facilitate the triiodide reduction reaction on the F_r CE. In contrast, the F_s CE consists of many large near-spherical particles, which may result in an increase in the R_s as well as the average current carrier transport length before reaching the site for triiodide reduction.[19] Meanwhile, with irregular surfaces, the electrons or holes must move through many interfaces before they can meet and recombine with each other,[10] which may result in the inferior electrocatalytic activity of F_s. However, the F_s CE is also covered with single sphere-shaped particles that may be active sites to improve the electrocatalytic activity. As a consequence, the F_s CE still exhibits good electrocatalytic activity.

In conclusion, we have shown that $FeSe_2$ films with controllable morphologies (including 3D flower-like and sphere-shaped) can be used as electrocatalysts for triiodide reduction in DSSCs. The F_r CE has been successfully demonstrated to be an efficient electrocatalyst with low charge-transfer resistance (R_{ct}) and fast reaction rates for the reduction of I_3^- ions, even slightly superior to Pt. As a consequence, the DSSC with the 3D flower-like $FeSe_2$ CE shows an η of 8.00%, slightly higher than that of the DSSC using a Pt CE (7.87%). In contrast, the F_s CE is inferior to the F_r CE. Furthermore, the simple preparation procedure and inexpensive cost properties of the $FeSe_2$ CE allow the development of a high-performance $FeSe_2$ CE to replace the expensive Pt CE catalyst in large-scale industrial DSSC production.

This work was financially supported by the National Basic Research Program of China under Grant No. 2011CBA00700, the National High Technology Research and Development Program of China under Grant No. 2010AA050510.

Notes and references

1 M. Gratzel, *Acc. Chem. Res.*, 2009, **42**, 1788–1798.
2 N. Papageorgiou, W. F. Maier and M. Gratzel, *J. Electrochem. Soc.*, 1997, **144**, 876–884.
3 K. S. Lee, W. J. Lee, N. G. Park, S. O. Kim and J. H. Park, *Chem. Commun.*, 2011, **47**, 4264–4266.
4 S. Ahmad, J. H. Yum, X. X. Zhang, M. Gratzel, H. J. Butt and M. K. Nazeeruddin, *J. Mater. Chem.*, 2010, **20**, 1654–1658.
5 X. J. Zheng, J. H. Guo, Y. T. Shi, F. Q. Xiong, W. H. Zhang, T. L. Ma and C. Li, *Chem. Commun.*, 2013, **49**, 9645–9647.
6 M. X. Wu, X. Lin, Y. D. Wang, L. Wang, W. Guo, D. D. Qu, X. J. Peng, A. Hagfeldt, M. Gratzel and T. L. Ma, *J. Am. Chem. Soc.*, 2012, **134**, 3419–3428.
7 F. Gong, X. Xu, Z. Q. Li, G. Zhou and Z. S. Wang, *Chem. Commun.*, 2013, **49**, 1437–1439.
8 F. Gong, H. Wang, X. Xu, G. Zhou and Z. S. Wang, *J. Am. Chem. Soc.*, 2012, **134**, 10953–10958.
9 M. K. Wang, A. M. Anghel, B. Marsan, N. L. C. Ha, N. Pootrakulchote, S. M. Zakeeruddin and M. Gratzel, *J. Am. Chem. Soc.*, 2009, **131**, 15976–+. Q9
10 Y. C. Wang, D. Y. Wang, Y. T. Jiang, H. A. Chen, C. C. Chen, K. C. Ho, H. L. Chou and C. W. Chen, *Angew. Chem., Int. Ed.*, 2013, **52**, 6694–6698.
11 A. I. Popov and D. H. Geske, *J. Am. Chem. Soc.*, 1958, **80**, 1340–1352.
12 G. Boschloo and A. Hagfeldt, *Acc. Chem. Res.*, 2009, **42**, 1819–1826.
13 J. D. Roy-Mayhew, D. J. Bozym, C. Punckt and I. A. Aksay, *ACS Nano*, 2010, **4**, 6203–6211.
14 S. Biallozor and A. Kupniewska, *Electrochem. Commun.*, 2000, **2**, 480–486.
15 Y. Saito, W. Kubo, T. Kitamura, Y. Wada and S. Yanagida, *J. Photochem. Photobiol., A*, 2004, **164**, 153–157.
16 A. Hauch and A. Georg, *Electrochim. Acta*, 2001, **46**, 3457–3466.
17 N. Koide, A. Islam, Y. Chiba and L. Y. Han, *J. Photochem. Photobiol., A*, 2006, **182**, 296–305.
18 Y. Hou, D. Wang, X. H. Yang, W. Q. Fang, B. Zhang, H. F. Wang, G. Z. Lu, P. Hu, H. J. Zhao and H. G. Yang, *Nat. Commun.*, 2013, **4**. Q10
19 T. N. Murakami, S. Ito, Q. Wang, M. K. Nazeeruddin, T. Bessho, I. Cesar, P. Liska, R. Humphry-Baker, P. Comte, P. Pechy and M. Gratzel, *J. Electrochem. Soc.*, 2006, **153**, A2255–A2261.